Effects of incident field refraction on scattered field from vertically extended cylindrical targets in range-dependent ocean waveguides

Elizabeth T. Küsel and Purnima Ratilal
Department of Electrical and Computer Engineering, Northeastern University, Boston, Massachusetts 02115

(Received 9 September 2008; revised 26 January 2009; accepted 27 January 2009)

The effect of incident field refraction on the scattered field from vertically extended cylindrical targets is investigated. A theoretical model for the total scattered field from a cylindrical target in a range-dependent ocean waveguide is developed from Green's theorem. The locally scattered field on the target surface is estimated as a function of the incident field by applying the appropriate boundary conditions on continuity of acoustic pressure and normal velocity, making the model applicable to general penetrable cylinders. The model can account for depth dependence in medium sound speed and hence refraction in the incident field along the target depth. Numerical implementation is done for a passive acoustic reflector, a long cylindrical air-filled rubber hose, often deployed vertically in experiments to provide calibration and charting consistency for wide-area active sonar systems. Analysis with the model indicates that refraction in the incident field along the target depth must be taken into account to accurately estimate the scattered field level from vertically extended cylindrical targets. It is demonstrated that the standard Ingenito waveguide target scattering model, which assumes that the incident field is planar along the target extent, can lead to significant errors of 10 dB or more in estimating the scattered field level.
 [DOI: 10.1121/1.3083235]

PACS number(s): 43.30.Gv, 43.20.Fn [WLS] Pages: 1930–1936

I. INTRODUCTION

In real ocean waveguides, the water column sound speed profile can vary significantly as a function of depth leading to acoustic field propagation that is highly refractive. Here, we investigate the effect of non-planar incident field on the scattered field from finite vertically extended cylindrical targets in range-dependent ocean waveguides. To better quantify the effect, we develop a theoretical model for the scattered field from a vertically extended cylindrical target that accounts for non-planar incident field over the target depth by direct application of Green's theorem.[1,2] The locally scattered field on the target surface at each depth is estimated as a function of the incident field by applying the boundary conditions on continuity of acoustic pressure and normal velocity, making the model applicable to general penetrable cylinders. Since the scattering contributions are calculated at each depth of the target, the object does not need to be located in an iso-speed layer. Furthermore, the scattering model for vertically extended cylindrical targets developed here can be implemented using both normal modes and the parabolic equation (PE) acoustic propagation models making the approach applicable to general range-dependent environments.[3,4]

The formulation is applied to calculate the scattered field from a cylindrical target[5] manufactured by BBN Systems and Technologies (Cambridge, MA) in several shallow water environments with different sound speed profile and bathymetry. The BBN target is often deployed during acoustic experiments[6,7] serving as a passive acoustic reflector for its known high target strength. Experiments that have deployed the BBN target include the ONR-sponsored 2006 Ocean Acoustic Waveguide Remote Sensing (OAWRS) Experiment at Georges Bank in the Gulf of Maine, and the 2001[8,9] and 2003 (Ref. 10) Acoustic Clutter Imaging Experiments in the New Jersey Strataform under the ONR Geoclutter Program. The BBN target is essentially a 30 m long and 7 cm diameter air-filled cylindrical hose made of gum rubber, suspended vertically off the seafloor at specified depths using a combination of anchors and floats. It provides a means to validate full-field waveguide scattering models and to minimize charting errors in range and bearing for active sonar systems. The scattered field from the BBN targets can also be compared to that from other targets of interest, such as fish schools, underwater vehicles, and the sea bottom, in order to determine their relative target or scattering strengths.

The scattering of sound by an object in an ocean waveguide is complicated due to multi-modal propagation and dispersion. The ocean-acoustic standard, Ingenito[11] waveguide target scattering model, is a widely used method[12–15] to calculate the single scattering from arbitrary sized objects in a horizontally stratified ocean waveguide. This approach is based on normal mode theory and it decomposes the incident field at the target center into modal plane waves. The object's plane wave scatter function is used to couple the incident and scattered modes which are then propagated to the receiver. The Ingenito model is therefore valid for large scatterers, large compared to the acoustic wavelength, in an ocean waveguide. However, it only applies to objects contained within an iso-speed layer because of modal plane wave decomposition at the target center. The Ingenito model cannot account for changes in medium sound speed along the target depth and assumes that the incident field is planar over the

 0001-4966/2009/125(4)/1930/7/$25.00

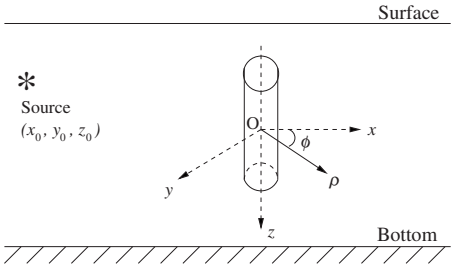

FIG. 1. Geometry of the scattering problem from a vertically extended cylindrical target of radius a and length L. The origin of the coordinate system is at the center of the cylinder.

target extent. Other approaches[16–22] for modeling object scattering in a waveguide are similarly limited, applicable to or implemented only for objects contained in an iso-speed layer. Some models[16,17,23–26] are only valid for horizontally stratified range-independent environments while others, such as the sonar equation,[27] are only valid for compact scatterers,[28] small compared to the acoustic wavelength, in a waveguide.

The theoretical vertically extended cylindrical target waveguide scattering (VETWS) model developed here is first calibrated against the Ingenito[11] model for the BBN target in a Pekeris waveguide where the target is contained within the iso-speed water column layer. The two models lead to scattered field levels as a function of range that match perfectly in this environment. The VETWS model is then implemented in a waveguide with the highly refractive water-column sound speed profile from the Gulf of Maine. In this environment, the BBN target extends over a depth where the water-column sound speed cannot be approximated as a constant and the field incident on the target is highly nonplanar. We show that when the Ingenito model is applied in this environment, it leads to significant errors of 10 dB or more in estimating the scattered field level for the BBN target.

Section II presents the theoretical approach and analytical formulation used to model the scattered field from a finite vertically extended cylindrical target in a general ocean waveguide. In Sec. III we describe the numerical implementation for the BBN target, and present results of calculations in both range-independent and range-dependent shallow water environments with different sound speed profiles. We compare the scattered field level using our model with that from the Ingenito model for each case.

II. THEORETICAL FORMULATION

In this section we develop the analytic formulation for the scattered field from a vertically extended cylindrical target in a range-dependent ocean waveguide. The origin of the coordinate system is placed at the target center with the z-axis pointing vertically downward and aligned with the axis of the cylinder, as shown in Fig. 1. The coordinates for points on the target are denoted by $\vec{r}_t=(x_t,y_t,z_t)=(\rho_t\cos\phi_t,\rho_t\sin\phi_t,z_t)$. Given a time harmonic source at location $\vec{r}_0$ and receiver at location $\vec{r}$, the total scattered field from the target is obtained by application of Green's theorem

$$P_{\text{scat}}(\vec{r})=-\oint_S [P(\vec{r}_t)\nabla_t G(\vec{r}|\vec{r}_t)-\nabla_t P(\vec{r}_t)G(\vec{r}|\vec{r}_t)]\cdot\vec{n}_t dA_t. \tag{1}$$

In Eq. (1), integration is performed over the surface S of the scatterer, $P(\vec{r}_t)$ is the total acoustic pressure on the target surface, $G(\vec{r}|\vec{r}_t)$ is the waveguide Green's function, and $\vec{n}_t$ is the unit vector normal to the surface of the object pointing away from the medium. Equation (1) is applicable to general targets with arbitrary boundary conditions.

The total pressure field on the surface of the target can be written as the sum of incident and scattered components

$$P(\vec{r}_t)=P_{\text{inc}}(\vec{r}_t)+P_{\text{scat}}(\vec{r}_t). \tag{2}$$

For a cylindrical target of radius $\rho_t=a$ and length L in an ocean waveguide, the local incident field on the surface of the target can be calculated numerically from an acoustic propagation model. The local scattered field on the surface of the cylindrical scatterer, on the other hand, is approximated in terms of Hankel functions as follows:

$$P_{\text{scat}}(\vec{r}_t)\approx\sum_{n=0}^{\infty}A_n(z_t)H_n^{(1)}(k(\vec{r}_t)\rho_t)\cos(n\phi_t). \tag{3}$$

At each depth point along the length of the target, this decomposition of the locally scattered field into cylindrical harmonics is valid since the acoustic mode cycle distances are typically much larger than the radius of the cylinder. In the above approximation, $H_n^{(1)}$ is the Hankel function of first kind and order n, and $k(\vec{r}_t)=\omega/c(\vec{r}_t)$ is the medium wavenumber, where ω is the circular frequency and $c(\vec{r}_t)$ is the range and depth-dependent medium sound speed. The depth-dependent coefficients $A_n(z_t)$ are optimally obtained by a least squares inversion applying the appropriate boundary condition at the surface of the target.

We assume that the radius of the cylinder is small compared to its length so that scattering is dominated by contributions from the curved surface of the cylinder and the contribution from the end caps is negligible. This also ensures that single scattering dominates for the vertically extended cylinder and multiple scattering with the waveguide boundaries is negligible.[29]

Next we examine three different boundary conditions for the finite vertically extended cylinder, the pressure-release, rigid, and penetrable surfaces.

A. Pressure-release target

The pressure-release condition states that the total pressure field at the target surface given by Eq. (2) must vanish. Substituting $P(\vec{r}_t)=0$ into Eq. (1) we observe that the first term under the integral sign goes to zero, and we obtain a simplified form for the total scattered field

$$P_{\text{scat}}(\vec{r})=\oint_S [\nabla_t P(\vec{r}_t)G(\vec{r}|\vec{r}_t)]\cdot\vec{n}_t dA_t. \tag{4}$$

In order to solve Eq. (4), we need to define the gradient of the local incident and local scattered pressure fields at the target surface. Over the curved surface of the circular cylinder,

$$\nabla_t P(\vec{r_t}) \cdot \vec{n_t} = -\frac{\partial P(\vec{r_t})}{\partial \rho_t}, \tag{5}$$

i.e., the gradient of the field dotted with the normal vector to the surface is just the derivative in the radial direction. The gradient of the incident field on the surface of the target can be calculated numerically from an acoustic propagation model. In order to calculate the gradient of the locally scattered field on the surface of the target, however, we first make use of Eq. (3) and the boundary condition to find the coefficients $A_n(z_t)$ and hence the local scattered field.

By substituting Eq. (3) and the pressure-release boundary condition into Eq. (2), we can write the resulting equation as a system of linear equations of the form

$$B\vec{q} = \vec{p} \tag{6}$$

at each depth point of the cylinder, where B is an $M \times N$ matrix of coefficients $H_n^{(1)}(k(\vec{r_t})\rho_t)\cos(n\phi_t)$, where M is the number of discrete points in azimuth around the cylinder and N is the number of terms of the Hankel function, $\vec{q}$ is the vector of coefficients $A_n(z_t)$ of length N we are interested in finding, and $\vec{p}$ is of size M and corresponds to $-P_{\text{inc}}(\vec{r_t})$, the negative incident pressure field at discrete azimuthal points around the cylinder. At each depth z_t of the target, we calculate the least-squares solution for $A_n(z_t)$ that minimizes $(\vec{p} - B\vec{q})$.

Once the coefficients $A_n(z_t)$ are determined and hence an approximation for the local scattered field, we use Eqs. (3) and (5) to calculate the gradient of the field as follows:

$$\frac{\partial P_{\text{scat}}(\vec{r_t})}{\partial \rho_t} = \sum_{n=0}^{\infty} A_n(z_t) H_n^{(1)'}(k(\vec{r_t})\rho_t)\cos(n\phi_t), \tag{7}$$

where $H_n^{(1)'}$ is the derivative of the Hankel function with respect to ρ_t expressed as[30]

$$\frac{\partial H_n^{(1)}(k(\vec{r_t})\rho_t)}{\partial \rho_t} = -k(\vec{r_t})H_{n+1}^{(1)}(k(\vec{r_t})\rho_t) + \frac{n}{\rho_t}H_n^{(1)}(k(\vec{r_t})\rho_t). \tag{8}$$

Substituting Eqs. (7) and (8), along with the gradient of the incident field and the waveguide Green's function into Eq. (4), we can calculate the scattered field from the pressure-release cylindrical target at any location in the waveguide. The summation in Eqs. (3) and (7) is truncated at N which is the maximum number of terms sufficient for accurately satisfying the boundary condition. However, since we are also calculating the gradient of the local scattered pressure analytically by Eq. (7), more terms may be needed in order to obtain a stable solution. For targets with small radius such that $ka \ll 1$, we expect only a few terms to be necessary in the approximations.

B. Rigid target

For a target with a rigid boundary, the radial component of the particle velocity must vanish at the surface

$$u(\vec{r_t}) = u_{\text{inc}}(\vec{r_t}) + u_{\text{scat}}(\vec{r_t}) = 0. \tag{9}$$

Note that on the surface of the circular cylinder, the radial component of the particle velocity and the total pressure are related by

$$u(\vec{r_t}) = -\frac{i}{\omega d(\vec{r_t})}\frac{\partial P(\vec{r_t})}{\partial \rho_t}, \tag{10}$$

where d is the medium density. Applying Eqs. (9) and (10) to Green's theorem in Eq. (1), the second term goes to zero and the total scattered field can be calculated from the simplified form below,

$$P_{\text{scat}}(\vec{r}) = -\oint_S [P(\vec{r_t})\nabla_t G(\vec{r}|\vec{r_t})] \cdot \vec{n_t} dA_t. \tag{11}$$

Equations (9) and (10) are used along with Eqs. (7) and (8) to find a least-squares solution for the depth-dependent coefficients $A_n(z_t)$ and the local scattered field. Once these quantities are computed, Eq. (11) is used to calculate the total scattered field at the receiver location.

C. Penetrable target

Let the region outside a homogeneous penetrable cylindrical target be called medium 1 and the region inside the target be called medium 2. The total pressure field in medium 1 is

$$P_1(\vec{r}) = P_{\text{inc}}(\vec{r}) + P_{\text{scat}}(\vec{r}), \tag{12}$$

where $P_{\text{inc}}(\vec{r})$ is calculated using a waveguide acoustic propagation model, as before, and $P_{\text{scat}}(\vec{r})$ is defined in Eq. (3). The pressure field inside the cylindrical target can be expressed as

$$P_2(\vec{r}) \approx \sum_{n=0}^{\infty} B_n(z_t) H_n^{(1)}(k(\vec{r_t})\rho_t)\cos(n\phi_t), \tag{13}$$

where the coefficients $B_n(z_t)$ are determined by application of the boundary conditions.

For this specific case, the two boundary conditions to be satisfied on the surface of the homogeneous penetrable cylindrical target are continuity of acoustic pressure, $P_1(\vec{r_t}) = P_2(\vec{r_t})$, and continuity of the radial component of particle velocity, $u_1(\vec{r_t}) = u_2(\vec{r_t})$. Applying these conditions to Eqs. (3) and (13), we obtain a system of equations that are optimally inverted to find the coefficients $A_n(z_t)$ of Eq. (3) and $B_n(z_t)$ of Eq. (13). Once these coefficients are determined, the total pressure field on the surface of the target can be calculated with Eq. (12) and its gradient with Eqs. (5), (7), and (8). Finally, Green's theorem, Eq. (1), is used to compute the total scattered field level at any location in the waveguide.

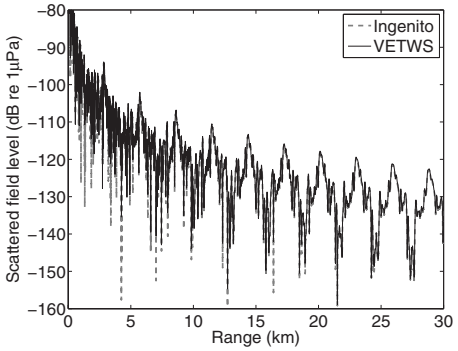

FIG. 2. Scattered field level from the BBN target in a 100 m deep Pekeris waveguide over sandy bottom of Example 1 calculated with the VETWS model and Ingenito model. Source of frequency 415 Hz is co-located with receiver at $z=50$ m; target is centered at $z=50$ m.

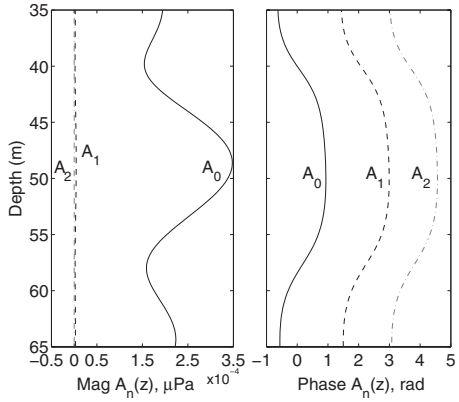

FIG. 3. Plot of magnitude and phase of coefficients $A_n(z_t)$ of Example 1 for target located at 20 km from 415 Hz source.

III. ILLUSTRATIVE EXAMPLES

We implement the scattering model derived in Sec. II for a $L=30$ m long BBN cylindrical target of radius $a=3.5$ cm. The air-filled BBN target satisfies a pressure-release boundary condition so that the equations in Sec. II A are used to compute the scattered field level. A normal mode model[31] is used to calculate the waveguide Green's function for the range-independent cases while the PE model[4] is used for the range-dependent environment. For all calculations, a monostatic configuration is used with a harmonic source of frequency either 415 or 950 Hz co-located with a receiver that measures backscattered fields from the cylindrical target. The acoustic wavelength is much larger than the target's radius, but smaller than its length. The geometry of the problem is shown in Fig. 1. In order to validate our model, we first compare the VETWS model results with Ingenito's scattering solution for the Pekeris waveguide. In addition, we also demonstrate the VETWS result in a layered waveguide with significant sound speed change as a function of target depth and in a range-dependent environment with downslope wedging bottom.

A. Range-independent cases

In order to implement the Ingenito[11,14] scattering model, the following scatter function for a pressure-release cylinder is used:[32,33]

$$S(\alpha,\beta;\alpha_i,\beta_i) = -\frac{kL}{\pi}\mathrm{sinc}\left[\frac{kL}{2}(\cos\alpha_i - \cos\alpha)\right] \times \sum_{m=0}^{\infty} B_m(-j)^m \cos(m[\beta-\beta_i]). \quad (14)$$

The above formula expresses the fact that the cylinder scatters in the vertical like a finite length array through the sinc function[32] and in azimuth through the cylindrical harmonics, where the amplitude of each harmonic for the pressure-release cylinder is given by

$$B_m = -\varepsilon_m j^m \frac{J_m(ka)}{H_m(ka)}. \quad (15)$$

In the above two equations, α and β correspond to the elevation and azimuth angles of the scattered plane waves, α_i and β_i correspond to the elevation and azimuth angles of the incident plane waves, ε_m is the Neumann number defined as $\varepsilon_0=1$, and $\varepsilon_m=2$ for $m\neq 0$, and J_m is the Bessel function of the first kind and order m.

We first compare the VETWS model with the Ingenito model for the BBN target in a 100 m deep Pekeris waveguide over a sandy bottom. The source, receiver, and target centroid are placed at $z=50$ m. The environmental parameters used in this example are water sound speed $c_w=1500$ m/s, bottom sound speed $c_b=1700$ m/s, bottom density $\rho_b=1.9$ g/cm^3, and bottom attenuation $\alpha_b=0.8$ dB/λ.

The total backscattered field level from the target as a function of source-target separation up to 30 km range for a source of frequency 415 Hz is shown in Fig. 2. As expected for this case where the object is contained in the iso-speed water column layer, the scattered levels calculated using the two methods are in very good agreement. Figure 3 shows the depth-dependent coefficients $A_n(z_t)$ of Eqs. (3) and (7) for the Pekeris waveguide problem when the target is located at r

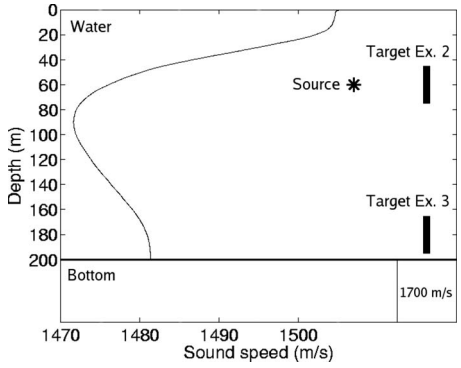

FIG. 4. Mean sound speed profile for Gulf of Maine, during September and October 2006, used in the calculations of the total scattered field for Examples 2 and 3. Source and target locations in depth for both examples are also shown for reference.

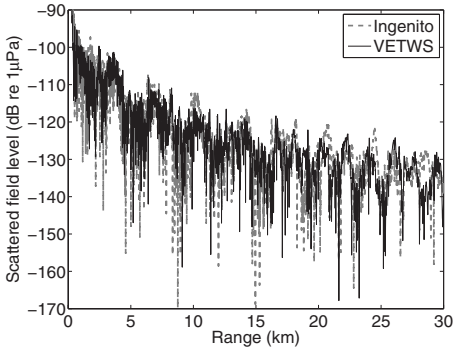

FIG. 5. Scattered field level from the BBN target in the depth-dependent waveguide scenario of Example 2 calculated with the VETWS model and Ingenito model. Source of frequency 415 Hz is co-located with receiver at $z=60$ m; target is centered at $z=60$ m.

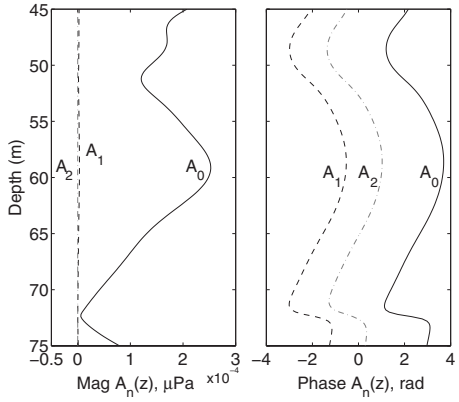

FIG. 6. Plot of magnitude and phase of coefficients $A_n(z_t)$ of Example 2 for target located at 20 km from 415 Hz source.

$=20$ km from the source. Note that only the first three terms in the sum of Eq. (7) are necessary to obtain a stable solution since $ka<0.1$.

Next, we examine the scattering from the BBN target in a 200 m deep waveguide with a depth-dependent sound speed profile over a flat sandy bottom. The sound speed profile used in the calculations, shown in Fig. 4, is the mean sound speed profile derived from 185 expendable bathythermograph measurements acquired during the OAWRS experiment in the Gulf of Maine between September and October 2006. For this environment, we consider two different source-receiver-target configurations illustrated in Fig. 4. In Example 2, the source and receiver are placed at $z=60$ m, and the target is centered at the same depth. In Example 3, the source and receiver are located at $z=60$ m, and the target is centered at $z=180$ m and is suspended 5 m off the bottom. For both examples, calculations are performed for two different frequencies.

In the geometry of Example 2, the target is contained within a layer where the medium sound speed change over the target depth is substantial, about 15 m/s. Figure 5 shows the level of the scattered field calculated using the VETWS model and Ingenito's model for Example 2 for a source of 415 Hz. In this case, the Ingenito model overestimates the scattered field level by roughly 3–5 dB. The modal interference structure of the scattered fields from the two models differ for this case. For the Ingenito model, the interference pattern for the scattered field level depends on the Green's function modal interaction with range at the target center. For the VETWS model, the interference pattern depends on the modal interaction integrated over the depth of the target. Furthermore, the Ingenito model does not account for changes in sound speed along the depth extent of the target. Instead, it uses the sound speed information at the center of the object and assumes that it is contained in an otherwise homogeneous layer. Our VETWS model, on the other hand, takes into account changes in medium sound speed and hence the incident acoustic field refraction along the depth extent of the target. The magnitude and phase of the coefficients $A_n(z_t)$ for Example 2 are shown in Fig. 6 for a target located at $r=20$ km from the 415 Hz source. Because of non-planar, refractive incident field over the target depth, the magnitude and phase of $A_n(z_t)$ in Fig. 6 vary much more drastically compared to Fig. 3 for the iso-speed Pekeris waveguide where these quantities vary smoothly over the target depth. The results for Example 2 using a source of frequency 950 Hz are similar to the lower frequency result, where the Ingenito model overestimates the scattered field level by roughly 3–5 dB.

The results for Example 3, in which the target is centered at $z=180$ m, are shown in Figs. 7(a) and 7(b) for the 415 and 950 Hz sources, respectively. Note that in this ex-

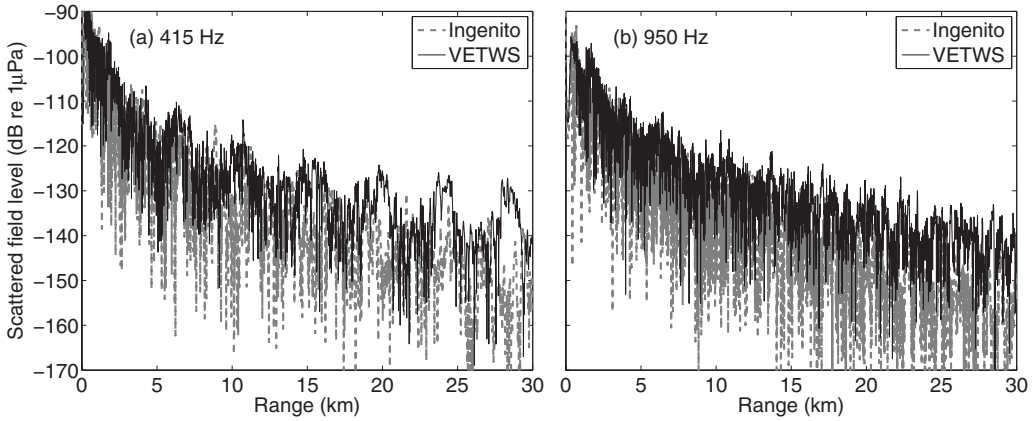

FIG. 7. Scattered field level from the BBN target in the depth-dependent waveguide scenario of Example 3 calculated with the VETWS model and Ingenito model. Source of frequency in (a) 415 Hz and in (b) 950 Hz is co-located with receiver at $z=60$ m; target is centered at $z=180$ m.

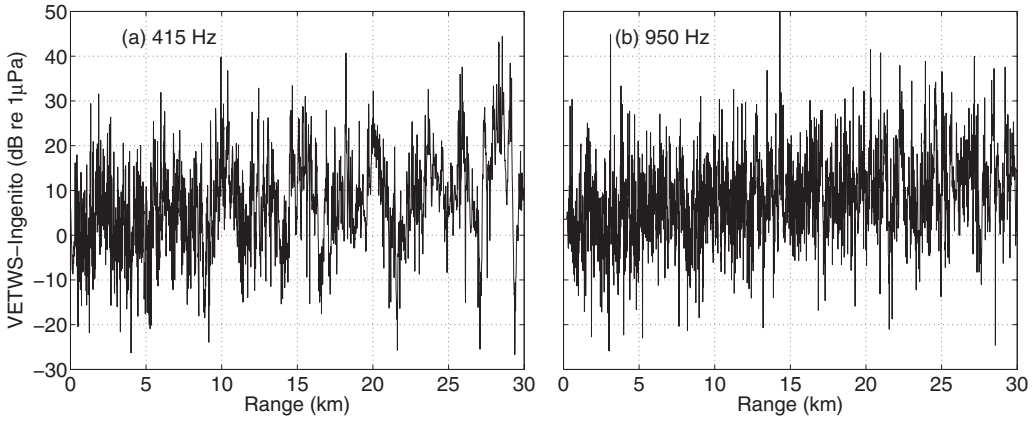

FIG. 8. Difference in scattered field level between the VETWS model and Ingenito model for Example 3 with target centered at $z=180$ m and sources of (a) 415 Hz and (b) 950 Hz.

ample, the target is contained within a layer where the medium sound speed changes by roughly 2 m/s over the target depth. For both frequencies the Ingenito model underestimates the scattered field level by more than 10 dB on average, beyond roughly 20 km source-target separation. The difference in the scattered field level from the VETWS and Ingenito models is shown in Figs. 8(a) and 8(b) for source frequencies of 415 and 950 Hz, respectively. We can observe from these plots that the difference between the two models increases on average with range for this source-receiver-target configuration.

B. Example in a range-dependent environment

In this section, the VETWS model is implemented with the PE to determine the total scattered field from the BBN target in a range-dependent environment. We consider the case of an iso-speed water layer with sound speed $c_w=1500$ m/s, over a downsloping wedge sandy bottom with sound speed $c_b=1700$ m/s. The bathymetry and sound speed used in this example are shown in Fig. 9. The source and receiver are placed at $z=50$ m, and the target is centered at the same depth. Figure 10 shows the total scattered field level for a source of frequency 415 Hz.

For comparison, we also apply the Ingenito model to calculate the total scattered field from the BBN target. Since Ingenito's model is implemented here using a range-independent normal mode model, we approximate the range-dependent waveguide as range-independent using the mean water depth, which in this case is 150 m. Other environmental parameters and the source-receiver-target configuration remain the same. The result is shown in Fig. 10 where we observe that the differences in the total scattered field between the correct range-dependent treatment of the waveguide and its approximation as range-independent are significant. Errors of over 10 dB for ranges greater than 10 km suggest the importance of our approach when calculating the scattered field from vertically cylindrical targets at long ranges from the receiver in real ocean environments.

In the future, the VETWS model developed here will be applied to examine the scattered field data from BBN targets deployed in the Gulf of Maine during the OAWRS experiment with a wide-area sonar in September to October 2006. The current model will be readily applicable to the highly range-dependent environment near Georges Bank where the targets were deployed. A stochastic propagation model will be used in conjunction with the VETWS model to take into account fluctuations in the medium and hence the observed scattered returns from the BBN target.

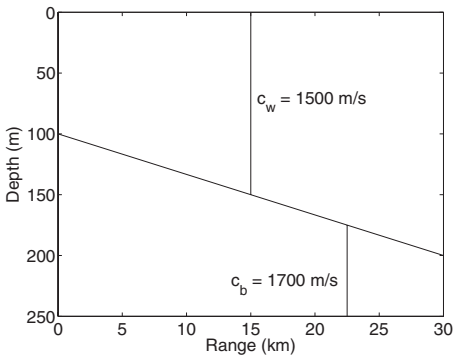

FIG. 9. Bathymetry and sound speed profile used in the calculations of the total scattered field for the range-dependent example.

IV. CONCLUSION

A theoretical model for the scattered field from a penetrable vertically extended cylindrical target in a range-

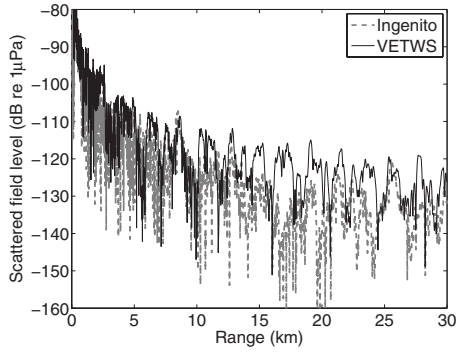

FIG. 10. Scattered field level from the BBN target in the range-dependent environment of Example 4 calculated with the VETWS model. Ingenito model is plotted as reference for a 150 m deep water column. Source of frequency 415 Hz is co-located with receiver at $z=50$ m; target is centered at $z=50$ m.

dependent ocean waveguide is developed from Green's theorem. The model takes into account changes in medium sound speed along the depth extent of the object and hence accounts for non-planar incident field on the target surface. The model is numerically implemented for the BBN target in several different shallow water waveguides. The BBN target is a thin and long air-filled rubber hose often deployed vertically during active acoustic imaging experiments at sea for accurate charting and sonar calibration. The model is validated against the Ingenito waveguide scattering model in an iso-speed Pekeris waveguide where both models lead to identical scattered field levels for the BBN target. In a realistic ocean waveguide, however, with significant change in medium sound speed over the target depth, our analysis shows that the Ingenito model can lead to errors of 10 dB or more in estimating the scattered field level. This is because the Ingenito model assumes that the incident wave over the extent of the target is planar. Our analysis indicates that changes in medium sound speed and hence refraction of the incident acoustic field along the depth extent of a vertically long target must be taken into account in order to accurately estimate its scattered field level in a general ocean waveguide.

ACKNOWLEDGMENTS

This work is funded by the Office of Naval Research, the National Oceanographic Partnership Program, and the Alfred P. Sloan Foundation, with administrative support from Bernard M. Gordon Center for Subsurface Sensing and Imaging Systems. This research is a contribution to the Census of Marine Life.

[1]P. M. Morse and K. U. Ingard, *Theoretical Acoustics* (Princeton University Press, Princeton, NJ, 1986).
[2]H. Medwin and C. S. Clay, *Fundamentals of Acoustical Oceanography* (Academic, San Diego, 1998).
[3]F. D. Tappert, *The Parabolic Approximation Method*, Lecture Notes in Physics Vol. **70** (Springer, New York, 1977).
[4]M. D. Collins, "A split-step Padé solution for the parabolic equation method," J. Acoust. Soc. Am. **93**, 1736–1742 (1993).
[5]C. I. Malme, "Development of a high target strength passive acoustic reflector for low-frequency sonar applications," IEEE J. Ocean. Eng. **19**, 438–448 (1994).
[6]W. M. Carey, P. G. Cable, W. L. Siegmann, J. F. Lynch, and I. Rozenfeld, "Measurement of sound transmission and signal gain in the complex Strait of Korea," IEEE J. Ocean. Eng. **27**, 841–852 (2002).
[7]S. Kim, W. A. Kuperman, W. S. Hodgkiss, H. C. Song, G. Edelmann, and T. Akal, "Echo-to-reverberation enhancement using a time reversal mirror," J. Acoust. Soc. Am. **115**, 1525–1531 (2004).
[8]Y. Lai, "Acoustic scattering from stationary and moving targets in shallow water environments with application to humpback whale detection and localization," Ph.D. thesis, Massachusetts Institute of Technology, Cambridge, MA (2004).
[9]P. Ratilal, Y. Lai, D. T. Symonds, L. A. Ruhlmann, J. R. Preston, E. K. Scheer, M. T. Garr, C. Holland, J. A. Goff, and N. C. Makris, "Long range acoustic imaging of the continental shelf environment: The Acoustic Clutter Reconnaissance Experiment 2001," J. Acoust. Soc. Am. **117**, 1977–1998 (2005).
[10]N. C. Makris, P. Ratilal, D. T. Symonds, S. Jagannathan, S. Lee, and R. W. Nero, "Fish population and behavior revealed by instantaneous continental shelf-scale imaging," Science **311**, 660–663 (2006).
[11]F. Ingenito, "Scattering from an object in a stratified medium," J. Acoust. Soc. Am. **82**, 2051–2059 (1987).
[12]J. S. Perkins, W. A. Kuperman, K. D. Heaney, and G. T. Murphy, "Scattering from an object in a three-dimensional ocean," in Proceedings of the 20th Annual International Meeting of the Technical Cooperation Subgroup, Subgroup G, Technical Panel 9 (1991).
[13]A. Sarkissian, "Extraction of a target scattering response from measurements made over long ranges in shallow water," J. Acoust. Soc. Am. **102**, 825–832 (1997).
[14]N. C. Makris and P. Ratilal, "A unified model for reverberation and submerged object scattering in a stratified ocean waveguide," J. Acoust. Soc. Am. **109**, 909–941 (2001).
[15]J. E. Quijano, L. M. Zurk, and D. Rouseff, "Demonstration of the invariance principle for active sonar," J. Acoust. Soc. Am. **123**, 1329–1337 (2008).
[16]R. H. Hackman and G. S. Sammelmann, "Acoustic scattering in an inhomogeneous waveguide: Theory," J. Acoust. Soc. Am. **80**, 1447–1458 (1986).
[17]G. S. Sammelmann and R. H. Hackman, "Acoustic scattering in a homogeneous waveguide," J. Acoust. Soc. Am. **82**, 324–336 (1987).
[18]N. C. Makris, "A spectral approach to 3-D object scattering in layered media applied to scattering from submerged spheres," J. Acoust. Soc. Am. **104**, 2105–2113 (1998).
[19]J. A. Fawcett, "A plane-wave decomposition method for modeling scattering from objects and bathymetry in a waveguide," J. Acoust. Soc. Am. **100**, 183–192 (1996).
[20]J. A. Fawcett, "Modeling acousto-elastic waveguide/object scattering with the Rayleigh hypothesis," J. Acoust. Soc. Am. **106**, 164–168 (1999).
[21]D. K. Dacol and D. G. Roy, "Wave scattering in waveguides," J. Math. Phys. **44**, 2133–2148 (2003).
[22]D. K. Dacol and D. G. Roy, "The partial-wave expansion for scattering in waveguides," J. Acoust. Soc. Am. **120**, 2518–2525 (2006).
[23]L. Cai, D. K. Dacol, D. C. Calvo, and G. J. Orris, "Acoustical scattering by arrays of cylinders in waveguides," J. Acoust. Soc. Am. **122**, 1340–1351 (2007).
[24]G. A. Athanassoulis and A. M. Prospathopoulos, "Three-dimensional acoustic scattering of a source-generated field from a cylindrical island," J. Acoust. Soc. Am. **100**, 206–218 (1996).
[25]G. A. Athanassoulis and A. M. Prospathopoulos, "All-frequency normal-mode solution of the three-dimensional acoustic scattering from a vertical cylinder in a plane-horizontal waveguide," J. Acoust. Soc. Am. **101**, 3371–3384 (1997).
[26]G. A. Athanassoulis and A. M. Prospathopoulos, "Three-dimensional acoustic scattering from a penetrable layered cylindrical obstacle in a horizontal stratified ocean waveguide," J. Acoust. Soc. Am. **107**, 2406–2417 (2000).
[27]R. J. Urick, *Principles of Underwater Sound*, 3rd ed. (McGraw-Hill, New York, 1983).
[28]P. Ratilal, Y. Lai, and N. C. Makris, "Validity of the sonar equation and Babinet's principle for scattering in a stratified medium," J. Acoust. Soc. Am. **112**, 1797–1816 (2002).
[29]A. Sarkissian, "Multiple scattering effects when scattering from a target in a bounded medium," J. Acoust. Soc. Am. **96**, 3137–3144 (1994).
[30]C. A. Balanis, *Advanced Engineering Electromagnetics* (Wiley, Hoboken, NJ, 1989).
[31]M. Porter and E. L. Reiss, "A numerical method for ocean-acoustic normal-modes," J. Acoust. Soc. Am. **76**, 244–252 (1984).
[32]H. C. van de Hulst, *Light Scattering by Small Particles* (Dover, New York, 1981).
[33]T. K. Stanton, "Sound scattering by cylinders of finite length. I. Fluid cylinders," J. Acoust. Soc. Am. **83**, 55–63 (1988).